NUMERICAL MODELLING OF WAVE OVERTOPPING EVENTS AT RUBBLE MOUND BREAKWATERS WITH A CREST ELEMENT

Mónica G. Aguilera Chaves[1], Marcel R.A. van Gent[1,2], Patricia Mares-Nasarre[2], Menno de Ridder[1,2]

Simulating the flow depths and velocities occurring during wave overtopping events at coastal structures with a numerical model is challenging. Reproducing these variables is relevant since they can be used as design parameters if they can be predicted accurately. OpenFOAM® was used to analyse flow depths and velocities that occur during wave overtopping events at a rubble mound breakwater with a crest element. The model was validated with physical model tests. Even though the quantitative prediction of the numerical model was not extremely accurate, the model provided valuable information to study the physical processes occurring during wave overtopping events. In particular, the effects of varying wave conditions and the protrusion height of the crest element have been studied. For events occurring with high exceedance probability, the flow depths and velocities follow the trends found by other authors who performed physical model tests. Flow depths and velocities that happen under complex flow phenomena still require further research.

Keywords: wave overtopping events; rubble mound breakwaters; crest element; flow depths; flow velocities; CFD; OpenFOAM®; waves2foam

INTRODUCTION

Climate change is causing sea level rise. A direct consequence is the increase in the overtopping discharges at coastal structures such as rubble mound breakwaters. This is caused not only by the sea level rise itself, but also by the consequent larger wave heights for structures with depth-limited design wave conditions. Larger and more frequent overtopping discharges threaten the safety of people, vehicles and other equipment at or behind the crest of coastal structures. Determining the flow depths (h_c) and velocities (u_c) that people and objects are able to withstand can be used as a method to design or adapt coastal structures. Some authors have already made efforts in this line in the past. For example, Abt et al. (1989), Jonkman & Penning-Rowsell (2008), Xia et al. (2014), Bae et al. (2016), and Sandoval et al. (2017) proposed threshold limits for human stability. Furthermore, equations have been proposed, based on physical model tests, to determine flow depths and velocities during wave overtopping events at the crest of coastal structures. For dikes see for instance Van Gent (2002), Schüttrumpf et al. (2002), Schüttrumpf and Van Gent (2003), and Van Bergeijk et al. (2019), and for rubble mound structures see for instance Mares-Nasarre et al. (2019, 2020, 2021, 2024) and Koosheh et al (2024). However, to establish design guidelines, flow depths and velocities need to be studied for a wide range of hydrodynamic conditions and coastal structure configurations. Although physical model tests can be used to fill this gap, they are expensive, and only a limiting number of tests can be performed in a campaign. Therefore, the equations derived from them have a limited range of validity. A time and cost-efficient alternative is the application of numerical models. Even though they need validation with physical model tests, they can be used to further explore results for configurations that were not analysed in the physical model tests. One of the most recent developments consists of the implementation of OpenFOAM® (Weller et al. 1998) with the waves2foam package (Jensen et al. 2014). OpenFOAM® has already been used to model wave overtopping over simple and complex coastal structures (e.g., Jensen et al. 2014; Chen et al. 2021, 2022; Irías Mata & Van Gent 2023). However, the capability of this tool to model flow depths and velocities has been less explored. The aim of this paper is to offer a first assessment on the accuracy of this tool for the prediction of flow depths and velocities, specifically at the crest of a rubble mound breakwater with a crest element.

METHODOLOGY

Description of the physical model tests for validation

For the validation of the numerical model, physical model tests executed in the Delta Basin at Deltares, the Netherlands, were used. The configurations that were tested included a rubble mound breakwater a) with a protruding crest wall and without a berm, and b) with a protruding crest wall and with a berm (see Figure 1). The structure had a seaward slope of 1:2 and a rear slope of 1:1.5. Three layers formed the breakwater: a permeable core (D_{n50} = 6.5 mm), a filter layer (D_{n50} = 17 mm) with a

[1] Deltares, Delft, 2629 HV, The Netherlands
[2] Hydraulic Engineering, Delft University of Technology, Delft, 2628 CN, The Netherlands

thickness of $2D_{n50}$, and an armour layer (D_{n50} = 33 mm) with a thickness of $2D_{n50}$, where D_{n50} is the nominal median diameter of the stones. The crest wall was placed directly on top of the core material. The freeboard relative to the still water level was A_c = 97 mm and R_c = 150 mm, excluding and including the crest wall, respectively. The berm width was 500 mm and was placed 50 mm below the still water level. The width and position of the berm, and the crest wall height remained unchanged for all the tests. Since the numerical model to be validated was 2DV, the tests that were used for its validation consisted of long-crested normal incident waves. Significant incident wave heights (H_{m0}) of 0.08, 0.10, 0.12, 0.14 and 0.16 m, and two different wave steepness were considered (s_{op} = 0.015 and 0.04, where $s_{op} = 2\,H_{m0}/gT_p^2$). Irregular waves based on the JONSWAP spectrum with a peak enhancement factor of 3.3 were generated. At least 1,000 waves were generated for each test. The water depth was kept as h = 0.80 m. Therefore, only one freeboard was tested.

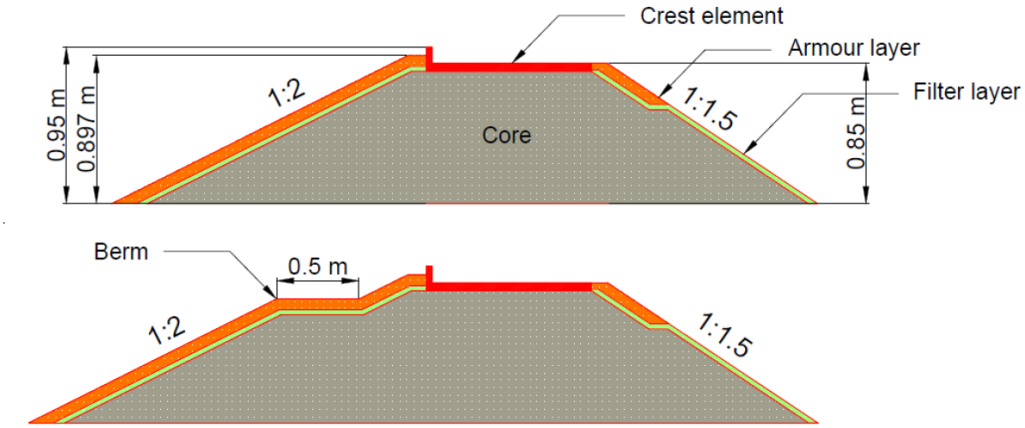

Figure 1. Rubble mound breakwater configurations used for the validation of the model.

To separate incident from reflected waves, directional wave gauges were positioned in front of the test sections of the structure, near the breakwater toe. The overtopping discharge was measured by collecting the overtopped water with overtopping boxes. Inside the boxes, wave gauges were installed to measure the water levels. The flow depths were measured with five layer thickness gauges that were located on the horizontal part of the crest wall. The flow velocities were estimated as the time it took for the wave front to move in between consecutive pins. Figure 2 shows the used measuring devices.

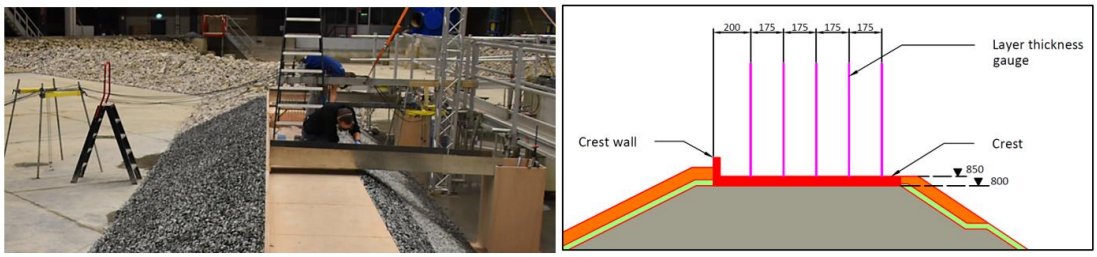

Figure 2. Measuring instruments used during the tests. The left panel shows one of the three wave gauges, and overtopping boxes. The layer thickness gauges are shown on the right panel. Dimensions in mm.

Description of the numerical model set-up

The numerical model was built in OpenFOAM® (Weller et al. 1998), a two-phase (air-water) Reynolds Averaged Navier-Stokes model, together with the package waves2Foam (Jensen et al. 2014). Waves2Foam uses the relaxation zone technique for the generation and absorption of waves (Jacobsen et al. 2012). It also employs the resistance-type porosity model by Jensen et al. (2014), which is based on Van Gent (1995), for the flow simulation inside the porous media. Tracking of the interface between air and water was effectuated with the Volume-of-Fluid approach (VOF) (Hirt & Nichols 1981). The VOF method uses the indicator function, F, to detect the interface. F is 0 for air, 1 for water, and holds a value in between for a mixture of the two fluids. The variant of VOF applied here was the one by Roenby et al. (2016) for its advantages in keeping a sharper interface between air and water, in avoiding wiggles around the free surface, and overestimation of velocities near the wave crests.

The height of the numerical flume was defined as 1.60 m, which is twice the water depth (0.80 m). At the bottom boundary and impermeable parts of the domain, a slip boundary condition was used. Relaxation zones were placed at the inlet and outlet boundaries of the domain to generate and absorb waves. The length of the relaxation zones was varied depending on the wave characteristics. In general, the length of the inlet and outlet relaxation zones was equal to one wave length and half the wave length based on the peak wave period and actual water depth. Six wave gauges were positioned between the end of the inlet relaxation zone and the toe of the breakwater to separate incident and reflected waves. They were located at 1.59 m, 1.91 m, 2.41 m, 3.01 m, 3.34 m and 4.04 m, from the breakwater toe for the configuration without the berm. The method by De Ridder et al. (2023) was used for this purpose. Figure 3 presents the final configuration of the numerical flume.

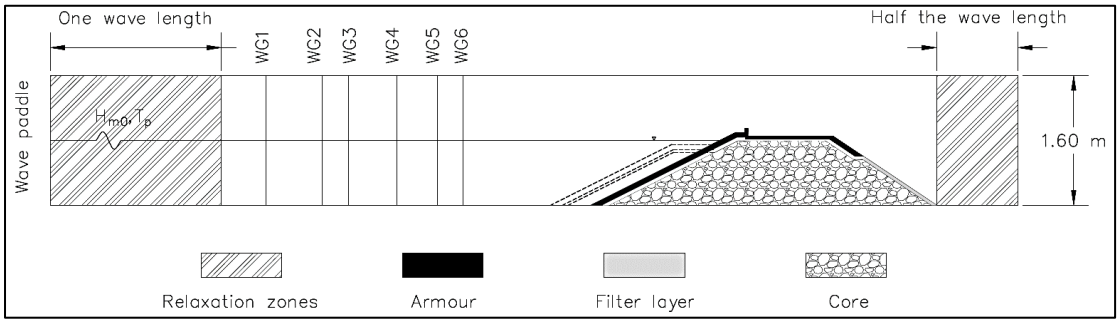

Figure 3. Layout of the numerical flume (coordinates and dimensions in meters).

The mesh was created by using the blockMesh and snappyHexMesh utilities of OpenFOAM®. The first one was used to generate the base mesh, while the second one was applied to refine the mesh in specified areas and to remove the crest wall from the model. The final grid configuration was based on a sensitivity analysis for convergence on wave propagation, and to accurately compute flow depths and velocities. Most of the base mesh consisted of squares of 40x40 mm. In the deeper parts of the water column, a grading was applied which increased the vertical dimension of the cells up to a factor of 1.25. Around the water level, the mesh was comprised by squares of 10x10 mm. Keeping an aspect ratio of 1 was relevant for a good representation of wave propagation and wave breaking (see Jacobsen et al. 2012). Consequently, the number of cells per wave height ranged between 8 and 16. Surrounding the crest wall, the grid was formed by squares of 5x5 mm, with a thickness of 20 mm. Figure 4 presents the final mesh.

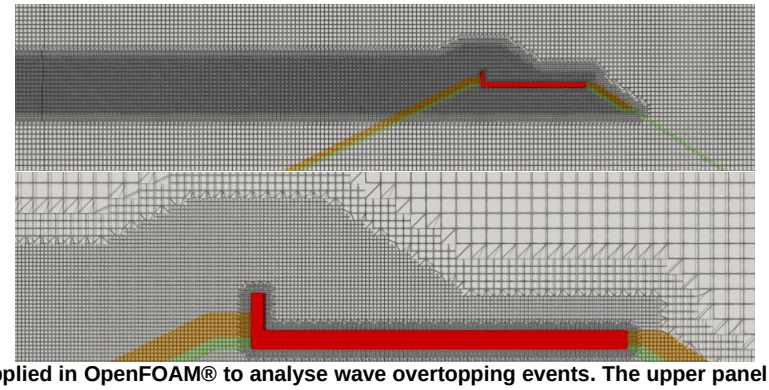

Figure 4. Grid applied in OpenFOAM® to analyse wave overtopping events. The upper panel shows the mesh in the whole numerical flume, and the lower panel shows the details of the mesh around the crest wall.

Since the physical model tests were carried out in a 3D environment, the wave-paddle velocity signal could not be used as model input. Instead, irregular waves were created through the inlet relaxation zone based on a JONSWAP spectrum with a peak enhancement factor of 3.3 (following a similar configuration as the physical model tests). The cosine stretching method and the split method were applied for the generation and evaluation of the wave signal for computational efficiency reasons (see Jacobsen 2017 for more detailed information about these methods). The input significant wave height was calibrated to obtain the target incident significant wave height at the position of the first numerical wave gauge (from left to right).

Following the approach by several authors (Van Gent 1995a, 1995b; Higuera et al. 2013a, 2013b; Jensen et al. 2014; Jacobsen et al. 2018; Molines et al. 2019; Irías Mata et al, 2023; Irías Mata & Van

Gent 2023), no detailed turbulence closure model was applied; a constant eddy viscosity was used instead. This approach is valid when little wave breaking occurs (such as the cases considered in this research), and because the turbulence effects inside the porous media are already accounted for in the resistance coefficients of the Darcy-Forchheimer equation. The resistance coefficients proposed in Van Gent (1995a), α_F = 1,000 and β_F = 1.1 were used as input for the simulations. In addition, a Keulegen-Carpenter number (KC, see Van Gent 1995a for the definition) of 10,000, a porosity value of 0.40, and D_{n50} values equal to the ones used in the physical model tests were assumed.

Wave overtopping was measured in the numerical flume by placing a discharge sheet ($\mathcal{E}$) on top of the crest wall (see Figure 5). This sheet was long enough to cover multiple cell faces (f). The flux of fluids (air and water) is captured through each of the cell faces. Then, each face fluid flux is multiplied by the fraction of water to obtain the overtopping discharge per cell face. The total discharge is the sum of the water fluxes through all the cell faces within the discharge sheet.

$$q^* = \sum_{f \in \mathcal{E}} \phi_{F,f} \frac{S_f}{\|S_f\|_2} \tag{1}$$

where S_f is the non-unit normal vector to the face, $\phi_{F,f}$ is the flux of water cross a face, and q^* is the instantaneous water flux in m^3/s. The reader is referred to Jacobsen (2017) for a more detailed explanation of the calculation method.

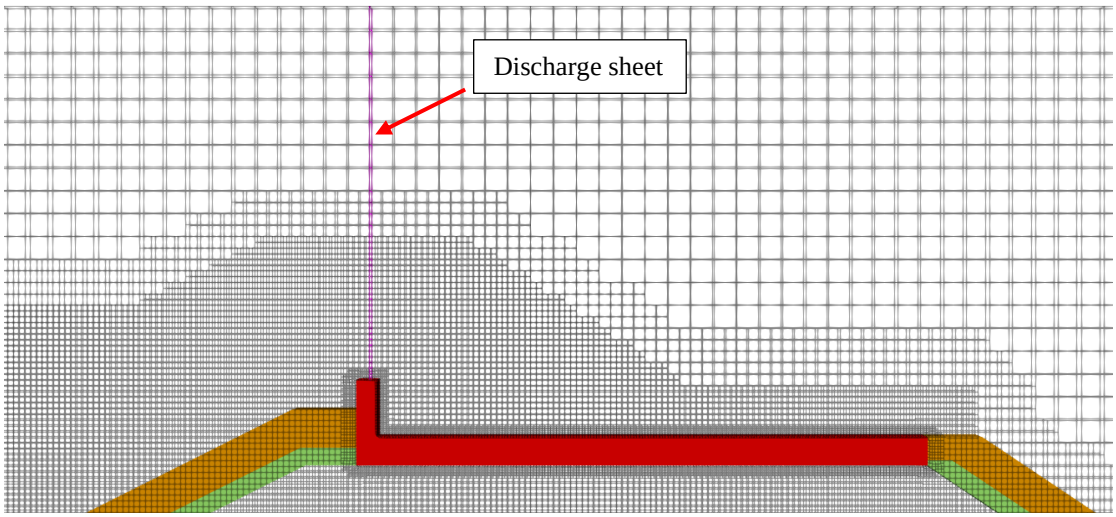

Figure 5. Discharge sheet used to capture the overtopping discharges during the simulations.

The numerical instruments used to obtain the flow depths and velocities were placed at 0.12 m intervals on and/or over the top of the horizontal part of the crest wall. The first one started 0.18 m after the vertical component of the L-shaped crest wall (see Figure 6). They had a different distribution with respect to the layer thickness gauges because, in the numerical model, the placement of these devices is limited by the mesh. Wave gauges were employed to extract the flow depths. Numerical wave gauges compress the water they find in the cells of their vertical plane as a single layer of water, and reference it with respect to the top of the horizontal part of the crest element. Three different methods were used to capture the flow velocities: a) with wave gauges and discharge sheets, b) with probes[3], and c) with planes[4]. From these, depth-averaged flow velocities were computed in a postprocessing step. For the first method, the overtopping discharge was divided by the flow depths to obtain the depth-averaged velocities. For the probes and planes, velocities in the x-direction were extracted at different elevations for the same horizontal position, but not further than 0.20 m above the top part of the horizontal component of the crest wall. It was assumed that these velocities were representative of a given depth (Δy), from which the depth-averaged velocities were computed according to the following equation:

$$u_{ci} = \frac{\sum_{j=1}^{j=N} u_{cji} * \Delta y_j * F_{ji}}{\sum_{j=1}^{j=N} \Delta y_j * F_{ji}} \tag{2}$$

[3] Probes in OpenFOAM® extract information from the numerical flume at points specified by the user. Their positioning is not restricted by the grid.

[4] Planes in OpenFOAM® can only be placed in cell faces. They extract information from the corners of the cell faces.

where u_c is the depth-averaged flow velocity, j represents each position in the y-axis where the velocities are extracted (for the same x-coordinate), N is the total number of extraction points in the y-axis, i indicates each computational timestep, Δy refers to the distance between consecutive extraction points in the vertical direction, and F is the indicator function of the VOF method.

In the case of the probes and planes, the velocities are extracted regardless of the fluid that is passing by. To correct for this, and to consider the velocities only for water, the indicator function was also extracted. Then, velocities extracted at the same time and position as an indicator function larger than 0.5 were further postprocessed. In addition, in Equation 2, the representative depth (Δy) was multiplied by the indicator function (F) to better approximate the real water layer for which a given velocity was representative of. Finally, from sensitivity analysis, it was determined that the first method (the one where wave gauges and discharge sheets were used) could not be trusted because it produced very high non-physical velocities. The probes and planes generated almost the same results, but the postprocessing took longer for the planes. For this reason, the probes were chosen as the option to carry out the final simulations.

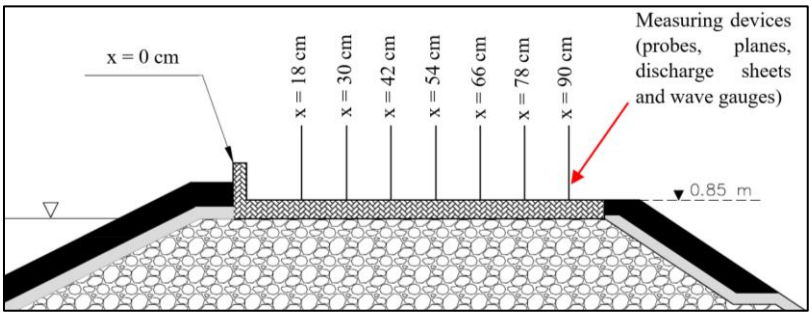

Figure 6. Set-up of numerical measuring devices. The position of the instruments is given in cm with respect to the vertical component of the L-shaped crest wall. The probes were located at a maximum height of 0.20 m above the horizontal component of the crest wall. Wave gauges and discharge sheets covered the entire vertical distance between the atmospheric boundary and the horizontal part of the crest element.

Method to analyse trends in flow depths and velocities

For the validation and sensitivity analysis on the flow depths and velocities, exceedance curves were computed. Separation of individual events was carried out in a similar fashion as the 'peak over threshold method'. No detailed statistical analysis to determine if the individual events were independent was performed. The threshold was varied for each simulated test and it was based on visual inspection.

Goodness of fit metrics to validate the numerical model

To evaluate the goodness of fit of computed values with respect to measured ones, two metrics, the Relative error and the Bias, were used. The lower the value of these indicators, the closer the computed values are to the measured ones. Equation 3 and Equation 4 present the mathematical definitions of the metrics.

$$\text{Relative error (\%)} = \left(\frac{\text{measured value} - \text{computed value}}{\text{measured value}}\right) * 100 \tag{3}$$

$$\text{Bias} = \frac{\sum_{i=1}^{n_{tests}} \left(\frac{\text{computed value}}{\text{measured value}}\right)}{n_{tests}} \tag{4}$$

VALIDATION OF THE NUMERICAL MODEL

In this section the model is validated in terms of its capability to reproduce incident waves, overtopping discharges, flow depths and flow velocities. 8 physical model tests were used to compare incident waves and overtopping discharges, and 6 physical model tests were used to compare the flow depths and velocities. To validate flow depths and velocities, it was necessary to obtain a statistically significant number of wave overtopping events, and the flow depths could not be extremely thin to avoid scale effects. For this reason, the set of tests to validate flow depths and velocities was different than the one used to validate incident waves and overtopping discharges. Each simulation consisted of at least 1,000 waves, as the physical model tests. Since the wave paddle velocity signal of the tests could not be used to create the waves in the numerical model, the comparison between modelled and measured incident waves, and overtopping discharge was performed statistically. The Relative error and Bias

between measured and computed values was estimated for the significant wave height (H_{m0}) and the spectral wave period ($T_{m-1,0}$). In case of the former, the Relative error ranged between -7.6% and 8.0%, with a Bias of 1.01. A fluctuation of the Relative error between positive and negative values indicates that there is no systematic overprediction or underprediction of the significant wave height. On the other hand, the relative error for the spectral wave period ranged between -8.8% and -1.6%, with a Bias of 1.05. In this case, all values were negative, which means that the computed spectral wave periods were always larger than the measured ones.

The validation of overtopping discharge prediction was carried out by comparing the non-dimensional mean wave overtopping discharge ($Q = q/(gH_{m0}^3)^{0.5}$) from the tests and the numerical simulations (see Figure 7). It is observed that the non-dimensional mean overtopping discharge is overpredicted for all the simulated tests except one. Overprediction of the mean wave overtopping discharges by OpenFOAM® has also been found in other studies (e.g., Chen et al. 2021; Irías Mata & Van Gent 2023). It can also be observed that the non-dimensional mean wave overtopping discharges are even larger with respect to the measured values in the cases where the berm is present. It seems that the numerical model is underpredicting the dissipation capacity of wave breaking and roughness of the berm. Underprediction of the berm dissipation was also found by Chen et al. (2021) for structures with a smooth slope. The bias was a factor 7.8, which indicates that the numerical model overpredicts the non-dimensional mean wave overtopping discharge by a factor 7.8 on average.

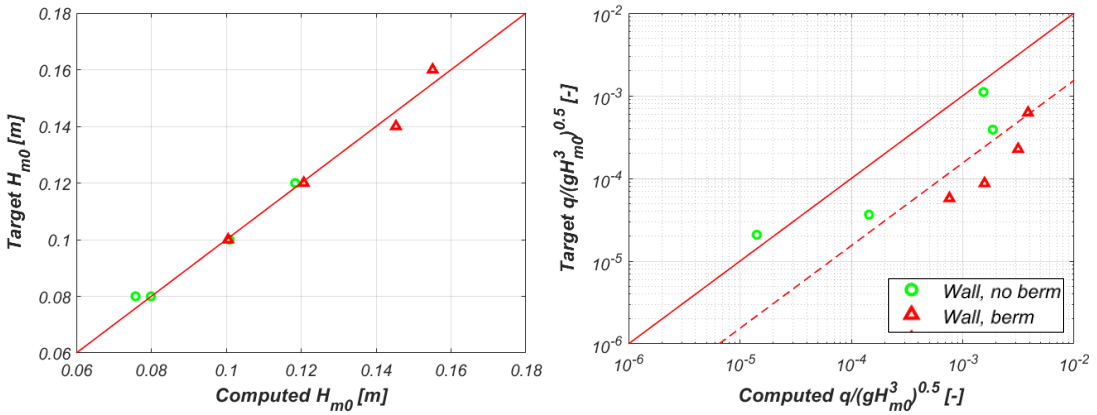

Figure 7. Left panel: Computed and measured wave heights. Right panel: Computed and measured non-dimensional mean wave overtopping discharges.

There are some possible causes for the overprediction of the numerical model of the mean wave overtopping discharge. The first one is related to the spectral wave periods ($T_{m-1,0}$), which were found to be larger when computed with the numerical model. A high spectral wave period generates a lower wave steepness, which causes larger mean wave overtopping discharges (see Van Gent et al. 2022; Irías Mata & Van Gent, 2023). The second reason is associated with the non-physical damping caused by the numerical model. It adds extra resistance which does not allow water to penetrate the porous media. Hence, water overtops the structure instead. This mechanism can be counteracted by calibrating the resistance coefficients of the Darcy-Forchheimer equation.

Exceedance curves were used to validate the flow depths and velocities. They were computed for the different positions at which the flow depths and velocities were extracted. Figure 8 presents an example for one of the tests. It is noted that the vertical lines that appear in the exceedance curves are a consequence of the threshold definition. Also, all the points plotted at 0 in the vertical axis appear because the exceedance curves are calculated based on the percentage of incoming waves (1,000). It can be observed that the trend, the magnitude, and number of events differs. The main cause for the discrepancies is the overprediction of the mean wave overtopping discharge. The evolution of the overtopping event might have also contributed to the differences. Particularly for the velocities, the computation method was not the same for the numerical model and the physical model tests (refer to the methodology section). Also, velocities in the negative x-direction were only taken into account in the numerical model. Regardless of the limitations in the estimations of the flow velocities, it is clear that numerical model is not accurate reproducing the magnitude of the flow depths and velocities. Despite this, the numerical model can still be used qualitatively to analyse physical processes that occur during wave overtopping events, and to assess effects of changing wave conditions and breakwater configurations on the flow depths and velocities.

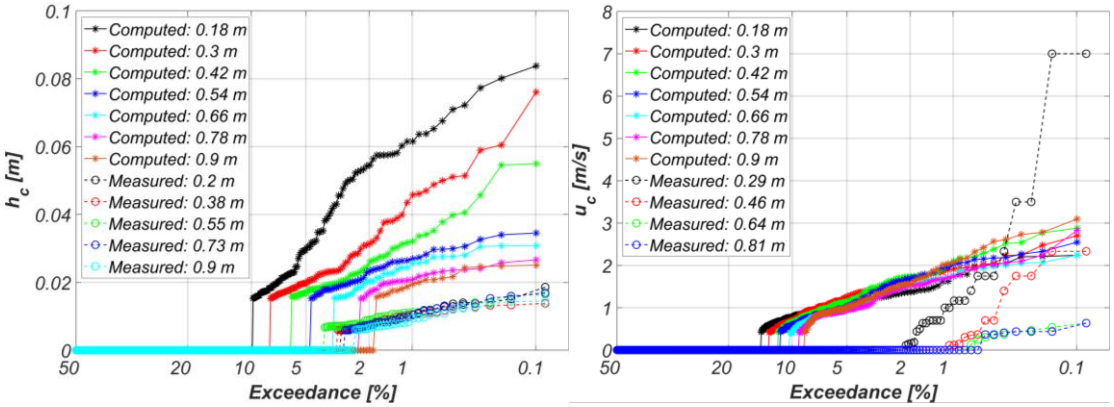

Figure 8. Comparison of exceedance curves obtained from the measured and simulated flow depths (left panel) and velocities (right panel) for one test (H_{m0} = 0.12 m and s_{op} = 0.04). The labels indicate the distance with respect to the vertical component of the L-shaped crest wall. The vertical lines appear due to the threshold definition. All points plotted at 0 in the vertical axis are a consequence of calculating the exceedance curve based on the percentage of incoming waves (1,000).

INFLUENCE OF PARAMETERS ON THE FLOW DEPTHS AND VELOCITIES

With the numerical model, varying protrusion heights of the crest wall (R_c-A_c) and wave conditions were examined to evaluate their influence on the flow depths and velocities. The breakwater configuration without the berm was used. To analyse the effect of changing wave conditions, three different significant wave heights (H_{m0} = 0.08, 0.12 and 0.16 m) were combined with three different wave steepness (s_{op} = 0.015, 0.027 and 0.04), leading to 9 simulations in total. The protrusion height was kept as in the original configuration (53 mm). Figure 9 presents the results in terms of exceedance curves for both the flow depths and velocities. The left panels show the results at different locations with respect to the vertical component of the L-shaped crest wall for a single wave condition (H_{m0} = 0.16 m and s_{op} = 0.027), and the right panels present the results for all simulated wave conditions for a single location (0.30 m landward from the vertical component of the L-shaped crest wall). The flow depths, regardless of the exceedance probability within the exceedance curves, decrease landward. The flow velocities show the same trend for high exceedance probability events. For low and medium exceedance probabilities (i.e. the more extreme events), the velocities increase the longer is the distance from the vertical part of the crest wall, until a point when they start to decrease. Furthermore, both the flow depths and velocities increase for higher incident significant wave heights and lower wave steepness. Similar trends were observed by other researchers who performed physical model tests on dikes, seawalls, and rubble mound breakwaters (e.g., Van Gent 2002; Cao et al. 2021; Mares-Nasarre et al. 2021). However, they always observed decreasing velocities for longer distances with respect to the seaside.

To study the impact of changing the protrusion height on the flow depths and velocities, 9 simulations were conducted with a constant significant wave height of 0.16 m, and with combinations of three different protrusion heights (R_c-A_c = 0 mm, 53 mm and 80 mm) with three different wave steepness (s_{op} = 0.015, 0.027 and 0.04). The results are shown in Figure 10, which zooms-in to one part of the exceedance curves to better capture the details. Note that the results are presented for only one location (0.66 m landward from the vertical component of the L-shaped crest wall). The region of high exceedance probabilities show that the flow depths and velocities are larger for smaller protrusion heights. This reflects the expected behaviour since a smaller protrusion height leads to more water overtopping the breakwater (see Van Gent et al. 2022; Irías Mata & Van Gent 2023). In addition, a smaller protrusion height leads to more (non-zero) events being captured in the exceedance curves. Despite the variation in the protrusion height, the flow depths and velocity trends with respect to the wave steepness are maintained; they increase for lower wave steepness. The trends shown for lower and medium exceedance probabilities do not follow the expected behaviour and require further research.

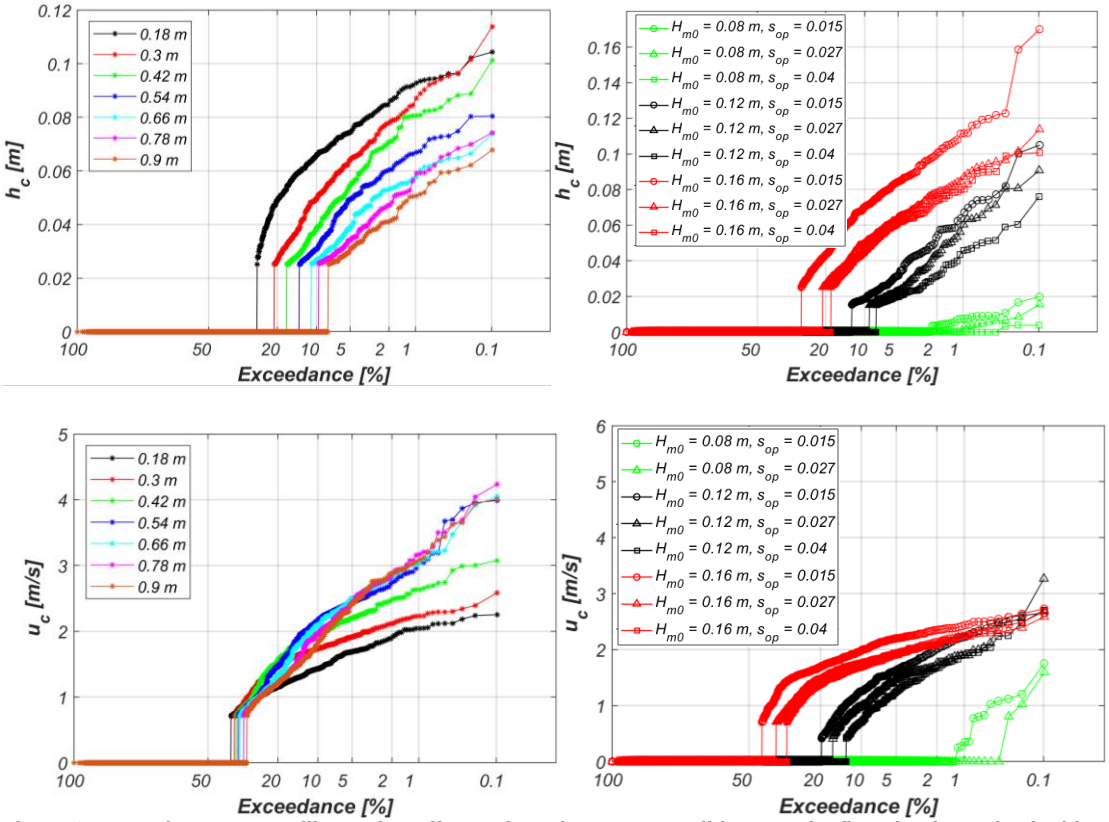

Figure 9. Exceedance curves illustrating effects of varying wave conditions on the flow depths and velocities. The upper left panel and the lower left panel show the flow depths and velocities at different distances with respect to the vertical component of the L-shaped crest wall for one wave condition (H_{m0} = 0.16 m and s_{op} = 0.027). The upper right panel and the lower right panel show the flow depths and velocities for all simulated wave conditions at one location (0.30 m landward from the vertical component of the L-shaped crest wall).

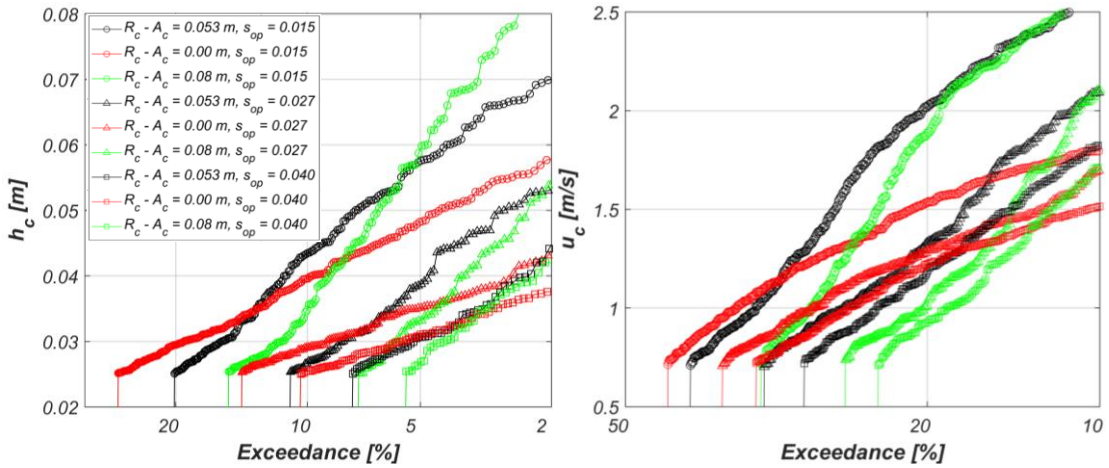

Figure 10. Exceedance curves illustrating effects of different protrusion heights and wave steepness on the flow depths and velocities (for H_{m0}= 0.16 m). Left panel: Flow depths; Right panel: Flow velocities. Both computed at 0.66 m landward from the vertical component of the L-shaped crest wall.

The hydrodynamics in the numerical flume were saved with a high frequency (e.g., each 0.05 s) to better analyse the physical processes. It was observed that once the events impact the horizontal part of the crest element, water gets accelerated to both the port side and the seaside (see Figure 11). As water propagates attached to and along the crest, friction acts upon it and the energy gets dissipated. The water that flows seaward moves while there is still water overtopping the breakwater. This seaward directed water later piles up against the vertical part of the L-shaped crest wall and returns towards the port side.

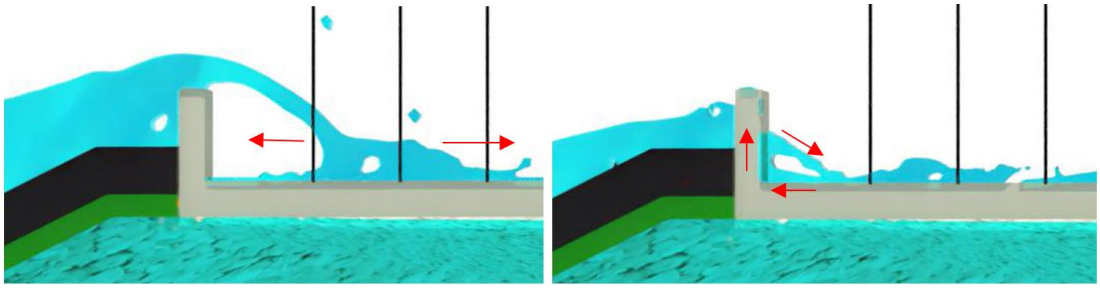

Figure 11. Computed flow after the impact. The left panel shows the water accelerating to the port and sea sides. The right panel shows water piling up against the vertical part of the crest wall and returning to the port side. The vertical black lines represent the position of measuring devices.

DISCUSSION

Some inconsistencies were found in the trends of the flow depths and velocities obtained from the numerical model when varying the wave conditions and protrusion heights of the crest wall. First, for moderate and high waves associated with low exceedance probabilities, the flow depths were physically larger than expected. Second, with the wave energy being dissipated by friction, the flow depths and velocities are expected to decrease landward. However, this was not always observed for the flow velocities (especially for medium and low exceedance probabilities). It was found that in these cases, the overtopping event hit the horizontal part of the crest element between the measuring devices (see left panel of Figure 11); thus, for the first measuring devices, the flow depths and velocities were extracted either before or just after the position of this impact. Also, as described above, after this impact the water gets accelerated to both the port and seaside. This acceleration causes a temporal increase in the velocity magnitude, especially towards the port side direction. In addition, at the time that water moves seaward, there is still water overtopping the breakwater. When depth-averaged, the positive velocities of the overtopping jet are to some extent compensated for by the negative velocities of the seaward flow. A higher protrusion just exacerbated these trends, since the events collided with the crest further landward than with a lower protrusion. Under these circumstances, the observed behaviour is different than for overtopping events when the entire overtopping flow remains attached to the horizontal part of the crest. Further examination is recommended for situations with overtopping jets generating flows in multiple directions.

Although not analysed in detail here, inaccuracies in the numerical model results may be caused by an underestimation of the energy dissipation due to wave breaking on the seaward slope, excessive resistance to the flow in the porous media due to numerical dissipation, and the presence of non-physical entrapped air in the model. Numerical dissipation in the porous media can be counteracted by calibrating the resistance coefficients of the Darcy-Forchheimer equation (see Irías Mata & Van Gent 2023). With respect to the non-physical entrapped air, Jacobsen et al. (2018) and Irías Mata et al. (2023) have already pointed out that entrapped air affects the estimated forces caused by wave impacts on the vertical component of the L-shaped crest wall. The wave interaction on the seaward slope, the permeability of the structure, and the wave interaction with the crest wall affect wave overtopping and hence affect the associated flow depths and velocities. In principle these parameters can all lead to large overtopping rates and, thus, wave overtopping jets can impact the horizontal component of the L-shaped crest wall further inland.

CONCLUSIONS AND RECOMMENDATIONS

In this research, a numerical model was set up using OpenFOAM® to simulate wave overtopping events at rubble mound breakwaters with a protruding crest element. Predicted incident waves and wave overtopping were compared to the measured values. Then, the numerical model was used to evaluate the accuracy of OpenFOAM® to reproduce the flow depths and flow velocities that occur during wave overtopping events. Overall, the model overpredicted the overtopping discharges, which also had repercussions on the accuracy of the modelled flow depths and velocities. However, the model proved to be valuable to further study the physical processes that take place during the overtopping events, in particular the effects of varying the wave conditions and protrusion height of the crest wall on the flow depths and flow velocities at the crest.

The numerical model can successfully reproduce expected trends in flow depths and flow velocities during wave overtopping events. It was observed that the flow depths and flow velocities increase for larger significant wave heights and lower wave steepness. The flow depth and flow velocities also generally decreased the longer the distance from the seaward boundary. These trends coincide with

observations by other studies on dikes and rubble mound breakwaters. However, the present study was focussed on structures with a protruding crest wall, and for these structures, similarities were only observed for events with a relatively high probability of exceedance. For these events the overtopping jet impacted the horizontal component of the L-shaped crest wall before the first measuring device. For positions more towards the port side, the flow remains attached to the horizontal part of the crest wall, which is comparable to the flow for dikes and breakwaters without a (protruding) crest wall. For more extreme events, with lower exceedance probabilities, the impact against the horizontal component of the crest element occurred between the measuring devices (further landward). In this case, the presence of the return flow affects the estimation of the flow depths and velocities. For these conditions the numerical model shows different trends than for the events with a high probability of exceedance. Since the most extreme events are the most dangerous ones for people, vehicles, or other equipment standing on or behind a breakwater crest, a more detailed analysis and future validation is still required. Also, it is necessary to improve the accuracy of the numerical model to obtain not only valuable qualitative results but also more accurate quantitative results. This can be achieved, for example, by matching wave overtopping discharges and collision points (with the horizontal part of the crest wall) to the associated measured values. It is also encouraged to evaluate if the presence of non-physical volumes of air has effects on the estimation of wave overtopping discharges, flow depths, flow velocities, and the position (collision point) where the overtopping jet reaches the horizontal part of the crest.

For future studies, it is advised to assess if there is an influence of the wave steepness on the collision point. In addition, more research is required to assess the dependencies of the flow depths and flow velocities on oblique waves. It is also paramount to determine if the model is capable of reproducing the trends found in literature (based on physical model tests), under more breakwater configurations (e.g., various seaward slopes, berm widths and berm levels, and the presence of a recurved parapet), and for various foreshore geometries with or without wave breaking on the foreshore. Furthermore, the shape of exceedance curves associated with exceedance probabilities lower than 2% remains to be verified (see Mares-Nasarre et al., 2024).

REFERENCES

Abt, S. R., Wittier, R. J., Taylor, A., & Love, D. J. (1989). Human stabillity in a high flood hazard zone. *Journal of the American Water Resources Association*, *25*(4), 881–890. https://doi.org/10.1111/j.1752-1688.1989.tb05404.x

Bae, H. U., Yun, K. M., Yoon, J. Y., & Lim, N. H. (2016). *Human stability with respect to overtopping flow on the breakwater*. *11*(1), 111–119.

Cao, D., Yuan, J., Chen, H., Zhao, K., & Liu, P. L.-F. (2021). Wave overtopping flow striking a human body on the crest of an impermeable sloped seawall. Part I: Physical modeling. *Coastal Engineering*, *167*, 103891. https://doi.org/10.1016/j.coastaleng.2021.103891

Chen, W., Warmink, J. J., Van Gent, M. R. A., & Hulscher, S. J. M. H. (2021). Numerical modelling of wave overtopping at dikes using OpenFOAM®. *Coastal Engineering*, *166*, 103890. https://doi.org/10.1016/j.coastaleng.2021.103890

Chen, W., Warmink, J. J., Van Gent, M. R. A., & Hulscher, S. J. M. H. (2022). Numerical investigation of the effects of roughness, a berm and oblique waves on wave overtopping processes at dikes. *Applied Ocean Research*, *118*, 102971. https://doi.org/10.1016/j.apor.2021.102971

De Ridder, M. P., Kramer, J., Den Bieman, J. P., & Wenneker, I. (2023). Validation and practical application of nonlinear wave decomposition methods for irregular waves. *Coastal Engineering*, *183*, 104311. https://doi.org/10.1016/j.coastaleng.2023.104311

Higuera, P., Lara, J. L., & Losada, I. J. (2013a). Realistic wave generation and active wave absorption for Navier–Stokes models. *Coastal Engineering*, *71*, 102–118. https://doi.org/10.1016/j.coastaleng.2012.07.002

Higuera, P., Lara, J. L., & Losada, I. J. (2013b). Simulating coastal engineering processes with OpenFOAM®. *Coastal Engineering*, *71*, 119–134. https://doi.org/10.1016/j.coastaleng.2012.06.002

Hirt, C. W., & Nichols, B. D. (1981). Volume of fluid (VOF) method for the dynamics of free boundaries. *Journal of Computational Physics*, *39*(1), 201–225. https://doi.org/10.1016/0021-9991(81)90145-5

Irías Mata, M., Boersen, S., Van Gent, M.R.A., Antonini, A., Jensen, B. & Van der Lem, C. (2023). A validation of wave loads on crest walls on top of composite breakwaters using OpenFOAM, *ASCE, Proc. ICCE 2022*, Sydney https://doi.org/10.9753/icce.v37.papers.23

Irías Mata, M., & Van Gent, M. R. A. (2023). Numerical modelling of wave overtopping discharges at rubble mound breakwaters using OpenFOAM®. *Coastal Engineering*, *181*, 104274. https://doi.org/10.1016/j.coastaleng.2022.104274

Jacobsen, N. G. (2017). *waves2Foam manual*.

Jacobsen, N. G., Fuhrman, D. R., & Fredsøe, J. (2012). A wave generation toolbox for the Open-Source CFD Library: OpenFoam®. *International Journal For Numerical Methods in Fluids*, *70*(9), 1073–1088.

Jacobsen, N. G., Van Gent, M. R. A., Capel, A., & Borsboom, M. (2018). Numerical prediction of integrated wave loads on crest walls on top of rubble mound structures. *Coastal Engineering*, *142*, 110–124. https://doi.org/10.1016/j.coastaleng.2018.10.004

Jensen, B., Jacobsen, N. G., & Christensen, E. D. (2014). Investigations on the porous media equations and resistance coefficients for coastal structures. *Coastal Engineering*, *84*, 56–72. https://doi.org/10.1016/j.coastaleng.2013.11.004

Jonkman, S. N., & Penning-Rowsell, E. (2008). Human Instability in Flood Flows. *JAWRA Journal of the American Water Resources Association*, *44*(5), 1208–1218. https://doi.org/10.1111/j.1752-1688.2008.00217.x

Koosheh, A., Etemad-Shahidi, A., Cartwright, N., Tomlinson, R. and Van Gent, M.R.A. (2024), Wave overtopping layer thickness on the crest of rubble mound seawalls. *Coastal Engineering*, https://doi.org/10.1016/j.coastaleng.2023.104441

Mares-Nasarre, P., Argente, G., Gómez-Martín, M. E., & Medina, J. R. (2019). Overtopping layer thickness and overtopping flow velocity on mound breakwaters. *Coastal Engineering*, *154*, 103561. https://doi.org/10.1016/j.coastaleng.2019.103561

Mares-Nasarre, P., Gómez-Martín, M. E., & Medina, J. R. (2020). Influence of Mild Bottom Slopes on the Overtopping Flow over Mound Breakwaters under Depth-Limited Breaking Wave Conditions. *Journal of Marine Science and Engineering*, *8*(1), 3. https://doi.org/10.3390/jmse8010003

Mares-Nasarre, P., Molines, J., Gómez-Martín, M. E., & Medina, J. R. (2021). Explicit Neural Network-derived formula for overtopping flow on mound breakwaters in depth-limited breaking wave conditions. *Coastal Engineering*, *164*, 103810. https://doi.org/10.1016/j.coastaleng.2020.103810

Mares-Nasarre, P., Van Gent, M.R.A. & Morales-Nápoles, O. (2024). A copula-based model to describe the uncertainty of overtopping variables on mound breakwaters, *Coastal Engineering*, https://doi.org/10.1016/j.coastaleng.2024.104483

Molines, J., Bayon, A., Gómez-Martín, M. E., & Medina, J. R. (2019). Influence of Parapets on Wave Overtopping on Mound Breakwaters with Crown Walls. *Sustainability*, *11*(24), 7109. https://doi.org/10.3390/su11247109

Roenby, J., Bredmose, H., & Jasak, H. (2016). A computational method for sharp interface advection. *Royal Society Open Science*, *3*(11), 160405. https://doi.org/10.1098/rsos.160405

Sandoval, C., Bruce, T., & Burgess, K. (2017). Wave overtopping hazard to pedestrians: Video evidence from real accidents. *Coasts, Marine Structures and Breakwaters 2017*, 501–512. https://doi.org/10.1680/cmsb.63174.0501

Schüttrumpf, H., Möller, J., & Oumeraci, H. (2002). Overtopping flow parameters on the inner slope of seadikes. *Proc. ICCE 2002*, 2116–2127. https://doi.org/10.1142/9789812791306_0178

Schüttrumpf, H. & Van Gent, M. R. A. (2003). Wave overtopping at seadikes, *Proc. Coastal Structures conference 2003*, Portland.

Van Bergeijk, V. M., Warmink, J. J., Van Gent, M. R. A., & Hulscher, S. J. M. H. (2019). An analytical model of wave overtopping flow velocities on dike crests and landward slopes. *Coastal Engineering*, *149*, 28–38. https://doi.org/10.1016/j.coastaleng.2019.03.001

Van Gent, M. R. A. (1995a). Porous Flow through Rubble-Mound Material. *Journal of Waterway, Port, Coastal, and Ocean Engineering*, *121*(3), 176–181. https://doi.org/10.1061/(ASCE)0733-950X(1995)121:3(176)

Van Gent, M. R. A. (1995b). *Wave interaction with permeable coastal structures.* [PhD thesis]. Delft University of Technology.

Van Gent, M. R. A. (2002). Wave overtopping events at dikes. *Coastal Engineering 2002*, 2203–2215. https://doi.org/10.1142/9789812791306_0185

Van Gent, M. R. A., Wolters, G., & Capel, A. (2022). Wave overtopping discharges at rubble mound breakwaters including effects of a crest wall and a berm. *Coastal Engineering*, *176*, 104151. https://doi.org/10.1016/j.coastaleng.2022.104151

Weller, H. G., Tabor, G., Jasak, H., & Fureby, C. (1998). A tensorial approach to computational continuum mechanics using object-oriented techniques. *Computers in Physics*, *12*(6), 620. https://doi.org/10.1063/1.168744

Xia, J., Falconer, R. A., Wang, Y., & Xiao, X. (2014). New criterion for the stability of a human body in floodwaters. *Journal of Hydraulic Research*, *52*(1), 93–104. https://doi.org/10.1080/00221686.2013.875073

APPENDIX

This section contains the list of symbols used throughout the article:

- $\mathcal{E}$: Used to indicate an overtopping discharge sheet in the expression that calculates flux of water through this element in OpenFOAM® [-].
- ϕ_F: Flux of water cross a face [m^3/s].
- A_c: Crest level of the armour with respect to the still water level [m].
- D_{n50}: Nominal median diameter of the stones [m].
- f: Representation of cell faces in expression used to estimate the flux of water through an overtopping discharge sheet in OpenFOAM® [-].
- F: Indicator function of the VOF method.
- g: Acceleration due to gravity [m/s^2].
- h: Water depth [m].
- h_c: Flow depth at the breakwater crest during wave overtopping events [m].
- H_{m0}: Incident spectral significant wave height, $H_{m0} = 4\sqrt{m_0}$ [m].
- KC: Keulegen-Carpenter number that considers the effect of the oscillatory flow in the Darcy-Forchheimer equation [-].
- q: mean overtopping discharge [$m^3/s/m$].
- Q: non-dimensional mean overtopping discharge [-].
- R_c: freeboard (including the height of the crest wall, if present) relative to the still water level [m].
- S_f: Non-unit normal vector to the cell faces used in the expression to estimate the flux of water through an overtopping discharge sheet in OpenFOAM® [-].
- s_{op}: Fictitious wave steepness. Wave steepness based on the wave height H_{m0} and the peak period T_p [-].
- $T_{m-1,0}$: spectral wave period based on the ratio of the spectral moments m_{-1} and m_0 of the incident wave spectrum [s].
- T_p: Peak period [s].
- u_c: Flow velocity at the breakwater crest during wave overtopping events [m/s].